Actin retrograde flow actively aligns and orients ligand-engaged integrins in focal adhesions

Vinay Swaminathan[a,b,c,1], Joseph Mathew Kalappurakkal[a,b,d,1], Shalin B. Mehta[e,1], Pontus Nordenfelt[a,b,f,g,h], Travis I. Moore[a,g,h], Nobuyasu Koga[i,j,k], David A. Baker[i,j], Rudolf Oldenbourg[e], Tomomi Tani[e], Satyajit Mayor[a,b,d,2], Timothy A. Springer[a,g,h,2], and Clare M. Waterman[a,b,c,2,3]

[a]Whitman Center, Marine Biological Laboratory, Woods Hole, MA 02543; [b]Physiology Course, Marine Biological Laboratory, Woods Hole, MA 02543; [c]Cell Biology and Physiology Center, National Heart, Lung, and Blood Institute, NIH, Bethesda, MD 20892; [d]National Centre for Biological Sciences, Bangalore 560065, Karnataka, India; [e]Eugene Bell Center, Marine Biological Laboratory, Woods Hole, MA 02543; [f]Division of Infection Medicine, Lund University, SE-221 84 Lund, Sweden; [g]Program in Cellular and Molecular Medicine, Children's Hospital, Boston, MA 02115; [h]Department of Biological Chemistry and Molecular Pharmacology, Harvard Medical School, Boston, MA 02115; [i]Department of Biochemistry, University of Washington, Seattle, WA 98195; [j]Howard Hughes Medical Institute, University of Washington, Seattle, WA 98195; and [k]Institute for Molecular Science, Okazaki 444-8585, Japan

Edited by David A. Weitz, Harvard University, Cambridge, MA, and approved August 21, 2017 (received for review January 20, 2017)

Integrins are transmembrane receptors that, upon activation, bind extracellular ligands and link them to the actin filament (F-actin) cytoskeleton to mediate cell adhesion and migration. Cytoskeletal forces in migrating cells generated by polymerization- or contractility-driven "retrograde flow" of F-actin from the cell leading edge have been hypothesized to mediate integrin activation for ligand binding. This predicts that these forces should align and orient activated, ligand-bound integrins at the leading edge. Here, polarization-sensitive fluorescence microscopy of GFP-αVβ3 integrins in fibroblasts shows that integrins are coaligned in a specific orientation within focal adhesions (FAs) in a manner dependent on binding immobilized ligand and a talin-mediated linkage to the F-actin cytoskeleton. These findings, together with Rosetta modeling, suggest that integrins in FA are coaligned and may be highly tilted by cytoskeletal forces. Thus, the F-actin cytoskeleton sculpts an anisotropic molecular scaffold in FAs, and this feature may underlie the ability of migrating cells to sense directional extracellular cues.

cell migration | mechanosensing | fluorescence polarization microscopy

Integrins are transmembrane cell surface receptors that mediate adhesion to the extracellular matrix (ECM) or other cells and signaling that directs proliferation, differentiation, and survival (1). Interaction of integrins with ligands is regulated such that high-affinity binding and signaling are induced by extracellular or intracellular cues in a process termed integrin activation (2). Activated integrins localize to focal adhesions (FAs), multimolecular plasma membrane-associated complexes that indirectly link ligand-bound integrins to the cytoskeleton through FA adapter proteins such as talin (3).

In addition to sensing ligands, integrins sense and promote responses to mechanical cues in a process called mechanotransduction (4). Cues include ECM stiffness, tension, or shear force, and can be inherently directional, as with tension and shear, or presented in gradients, as with ECM stiffness. These directional mechanical cues elicit behaviors such as polarization of endothelial cells in response to blood flow or cancer cell migration out of tumors (5–7). However, how integrins in FAs sense the direction of mechanical cues is not known.

The anisotropic intracellular mechanical environment and shape of FAs may underlie FA sensitivity to directional mechanical cues. The F-actin linked to integrins is anisotropic in its organization and dynamics. In migrating cells, integrins engage to ECM to form FAs at the leading edge, where actin filaments (F-actin) orient with their growing ends facing the plasma membrane (8). Polarized actin assembly pushes against the membrane, driving F-actin toward the cell center in a process termed "retrograde flow" (9). The forces of F-actin retrograde flow and myosin II contractility are transmitted through FA and integrins into traction on the ECM that drives the cell forward (10). The elongated shape of FAs results from force-dependent, directional recruitment of integrins and FA proteins along the axis of retrograde flow (8). Thus, polarized intracellular forces mediate FA growth and function in driving cell migration, suggesting that integrins and/or their activation may be intrinsically sensitive to directional force.

How could transmembrane receptors sense directional force? Cytoskeletal forces are thought to provide an ultrasensitive mechanism for triggering integrin activation by inducing structural transitions between inactive and active integrin conformations (11). This model for integrin activation, termed "the cytoskeletal force hypothesis," predicts that directional forces exerted on the integrin β-subunit through a talin-mediated linkage to F-actin would activate and orient integrins with the β-subunit toward and the α-subunit away from the direction of applied force (11). This implies a translation of F-actin retrograde flow into a molecular-level, direction-dependent activation and organization of membrane receptors and could underlie the directional mechanosensing of physical cues by integrins.

Here, we sought to test whether talin-mediated linkage of integrins to F-actin forces and subsequent activation and binding to an immobilized ligand orients and aligns activated integrins in FAs of migrating cells. We used engineered green fluorescent protein (GFP)-integrin chimeras and imaging with polarization-sensitive

Significance

Integrins are adhesion receptors linking cells to their environment, which function as sensors of physical and chemical information to regulate development, immune response, and vascular function. How integrins receive and transduce directional forces including flow or tissue tension has remained elusive. We used polarization-based microscopy techniques to discover that activated αVβ3 integrins are aligned with one another in focal adhesions in migrating fibroblasts. Integrin coalignment is sensitive to mechanical resistance of its ligand and coupling to a dynamic F-actin cytoskeleton, consistent with the "cytoskeleton force model" for integrin activation. Our work suggests that activated integrins are actively ordered at the molecular scale by cellular forces, which may underlie their ability to sense directional forces in their environment to mediate critical functions.

Author contributions: S.M., T.A.S., and C.M.W. designed research; V.S., J.M.K., S.B.M., and N.K. performed research; J.M.K., S.B.M., P.N., T.I.M., N.K., D.A.B., R.O., T.T., and T.A.S. contributed new reagents/analytic tools; V.S., J.M.K., S.B.M., P.N., and T.A.S. analyzed data; and V.S. and C.M.W. wrote the paper.

The authors declare no conflict of interest.

This article is a PNAS Direct Submission.

Freely available online through the PNAS open access option.

[1]V.S., J.M.K., and S.B.M. contributed equally to this work.

[2]S.M., T.A.S., and C.M.W. contributed equally to this work.

[3]To whom correspondence should be addressed. Email: watermancm@nhlbi.nih.gov.

This article contains supporting information online at www.pnas.org/lookup/suppl/doi:10.1073/pnas.1701136114/-/DCSupplemental.

fluorescence microscopy. We show that αVβ3 integrins are coaligned in FAs by F-actin flow, talin, and ligand binding. Rosetta modeling suggests that ligand-bound αVβ3 may be markedly tilted relative to the cell surface. This supports the cytoskeletal force hypothesis for integrin activation and suggests that the highly organized, anisotropic molecular scaffold of FAs may underlie the cells sensitivity and response to directional mechanical cues.

Results

To test the hypothesis that integrins are aligned in FAs by engagement to immobilized ligand and cytoskeletal flow, we used mouse embryonic fibroblasts (MEFs) coexpressing untagged β3 integrin together with GFP-αV integrin chimeras plated on the αVβ3 ligand fibronectin (FN) (*SI Materials and Methods* and Fig. 1*A*). To analyze ensemble GFP-integrin organization and mobility, we used emission anisotropy–total internal reflection fluorescence microscopy (EA-TIRFM) (Fig. 1*B*, *Top* and Fig. S1). Fluorescence excitation is plane polarized so that GFPs whose transition dipoles (henceforth called dipoles) are oriented parallel to the plane of excitation will be selectively excited. The parallel (I_{II}) and perpendicular ($I_{\perp}$) components of the emission are separated by a polarizing beam splitter onto two cameras (12) (Fig. 1*B*). If the GFPs are sterically constrained relative to the integrins and the integrins are immobile and coaligned such that the GFP dipole is parallel to the plane of polarization, the emission of the ensemble, averaged over the diffraction limit and camera exposure time will be collected mainly in the parallel channel, since the excitation and emission dipoles of GFP are nearly colinear (13). If the integrins are not immobile and coaligned, or the GFPs are not constrained relative to immobile and aligned integrins, the emission will not be biased to the parallel channel. Constrained GFPs in integrins that are coaligned but not oriented parallel to the excitation axis will be minimally excited. The relative intensities in the parallel and perpendicular channels thus reflect the coalignment and steric constraint of both, integrin and GFP.

To quantify GFP-integrin emission anisotropy (henceforth referred to as anisotropy), we defined a microscope coordinate system *XYZ*, where the *Z* axis is the optical path, the *X* and *Y* axes are in the microscope stage plane, and the plane of excitation polarization is along the *Y* axis (Fig. S1 *A*). The anisotropy (r) of the emission is $r = (I_{II} - I_{\perp})/(I_{II} + 2I_{\perp})$, where I_{II} is the emission component that is polarized parallel to the excitation, and $I_{\perp}$ is the intensity of the perpendicular component (Fig. S1 *B* and *C*). We validated results obtained by EA-TIRFM using Instantaneous FluoPolScope where the sample is illuminated with isotropic polarization and anisotropy is determined using detectors sensitive to four different emission polarization orientations (14) (Fig. 1*B*, *Bottom*).

To parse the effects of coalignment and steric constraint on anisotropy of integrins measured with EA-TIRFM, we generated two integrin-GFP chimeras with different degrees of constraint of GFP relative to αVβ3. In "αV-GFP-unconstrained," the N terminus of GFP was fused by a 9-aa flexible linker to the C-terminal cytoplasmic tail of αV integrin (Fig. 1*A*). This allows the orientation between integrin and the GFP dipole to be random such that any measured anisotropy is due to constraint or alignment imposed on GFP and/or integrin by the environment. The second chimera was designed to constrain the GFP relative to integrin (Fig. 1*A*), thus reporting on constraint and coalignment of the integrin itself (15). In αV-GFP–constrained, GFP was fused in frame to a β-loop between Lys-259 and Asn-260 in the β-propeller in the extracellular headpiece of αV, with the unstructured 5 aa at the N terminus and 3 aa in the C terminus of the GFP replaced with a structurally neutral two-residue linker (Fig. 1*A*). When expressed in MEFs, both αV-GFP chimeras concentrated at paxillin-mCherry–marked FAs, paired with β3 integrin (evidenced by immunofluorescence of αVβ3 with LM609 antibody), and had no effect on FA size or number (Fig. S2).

αV Integrins Are Coaligned and Oriented with Respect to the FA Long Axis. We then performed EA-TIRFM imaging to analyze integrin mobility and alignment. We expressed the integrin-GFP chimeras in MEFs and validated that anisotropy in FAs was independent of expression level, FA size, and FA location in the cell (Fig. S3 *A* and *B*). We used αV-GFP–unconstrained to analyze the effect of the FA environment on integrin-GFP mobility. This showed that anisotropy was low throughout the basal cell surface (Fig. 1*C*) except for within segmented FAs, where it was significantly higher than regions outside FAs (Fig. S3*C*). By contrast, either GFP-tagged membrane-targeting sequence (CAAX-GFP) or soluble GFP showed

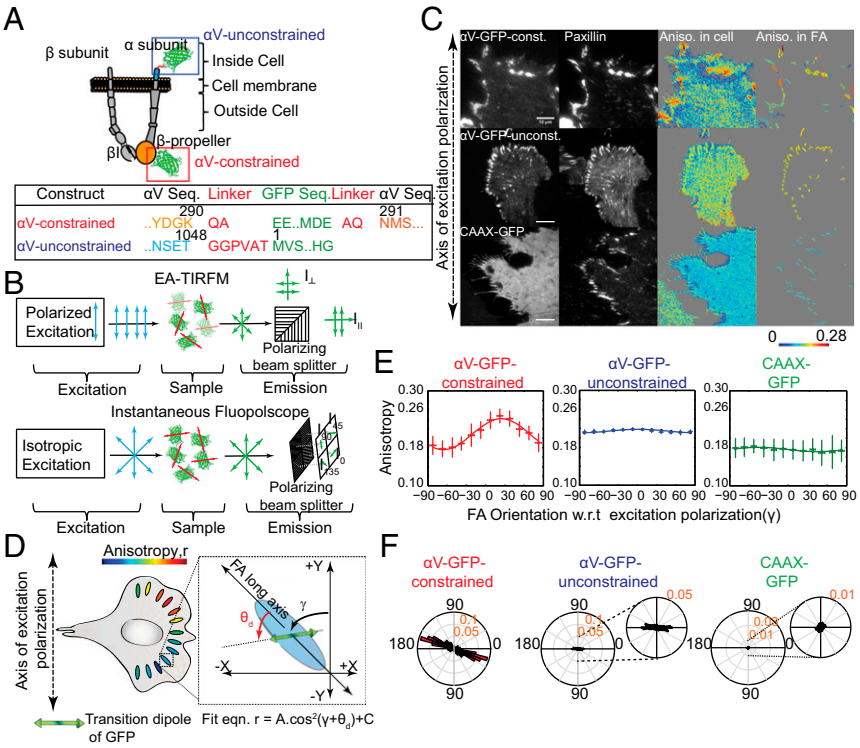

Fig. 1. αV integrins are aligned and oriented relative to the FA long axis. (*A*, *Top*) Schematic of αV-GFP constrained and unconstrained chimeras shown in extended-open αVβ3. (*A*, *Bottom*) Amino acid sequence at GFP-αV integrin junctions. (*B*) Schematic of EA-TIRFM (*Top*), Instantaneous FluoPolScope (*Bottom*). (*C*, *Left* and *Left Center*) Fluorescence images of αV-GFP-integrin chimeras (*Top Left* and *Center Left*), GFP-CAAX (*Bottom Left*) or mApple-paxillin (*Left Center*) in MEF plated on FN. Anisotropy magnitude (r) in cells (*Right Center*) and in FAs (*Right*) of αV-GFP or GFP-CAAX. Excitation polarization orientation (*Left*), anisotropy color scale (*Bottom*). (*D*) Schematic of average r in FAs of different orientation with respect to polarization axis (γ) if GFP dipoles were aligned in FA as in zoom. Fit equation (*Bottom*). (*E*) Average r in FAs vs. γ for GFP chimeras, overlaid with fit to function in *D*. Error bars represent SEM. (*F*) Histogram of GFP dipole orientation relative to FA long axis measured by Instantaneous FluoPolScope; concentric circles: polarization factor (p); 0–180° axis: FA long axis. $n_{\alpha V\text{-GFP-constrained}} = 164$ FAs, 5 cells; $n_{\alpha V\text{-GFP-unconstrained}} = 257$ FAs, 8 cells; $n_{CAAX\text{-}GFP} = 375$ FAs, 12 cells. (Scale bar, 10 μm.)

low anisotropy irrespective of localization relative to FAs (Fig. 1*C* and Fig. S3*C*). Thus, GFP-integrin mobility is constrained in FAs, in agreement with fluorescence recovery after photobleaching and single-molecule analyses (16, 17).

Next, we analyzed the anisotropy of the αV-GFP–constrained chimera. Similar to the αV-GFP–unconstrained chimera, αV-GFP–constrained showed higher anisotropy inside FA than outside FAs (Fig. 1*C* and Fig. S3*C*). However, in contrast to the unconstrained chimera where anisotropy was at a similar intermediate level in all FAs, the anisotropy for αV-GFP–constrained was highly variable between individual FAs in a cell, spanning the full dynamic range of the measurement (Fig. 1*C*). Thus, integrins in a subset of FAs have constrained mobility and their attached GFPs have their dipoles oriented parallel to the plane of excitation.

FAs themselves exhibit an anisotropic shape with the FA long axis generally oriented perpendicular to the leading edge. Examination of EA-TIRFM images of cells expressing αV-GFP–constrained suggested that FAs with similar orientations of their long axes with respect to the excitation polarization exhibited similar anisotropy, implying that integrins may be coaligned with respect to the FA long axis. This, in turn, predicted that αV-GFP–constrained anisotropy should vary as a function of the angle of the FA long axis with respect to the excitation plane (Fig. 1*D*).

To test whether integrins were coaligned relative to the FA axis, we fitted segmented FAs with an ellipse, determined the angle of the ellipse long axis relative to the plane of excitation polarization, and plotted average anisotropy in FAs as a function of FA orientation. This "radial sector analysis" confirmed that anisotropy varied as a function of FA orientation with respect to the plane of excitation, with peak anisotropy at approximately −15 to −30°, and minimum at ∼−60 to −75° (Fig. 1*E*). The anisotropy vs. FA orientation data were fitted to a $\cos^2$ function that is expected if dipoles are coaligned and orientated with respect to the FA long axis (Fig. 1 *D* and *E*): $r = C + A\cdot\cos^2(\gamma + \theta_d)$, where C is the isotropic background; A, the amplitude of peak-to-peak anisotropy modulation, is directly related to the fraction of sterically constrained and coaligned GFP dipoles; γ is the angle of the FA with respect to the excitation polarization axis, and θ_d is the angle of the GFP dipoles with respect to the FA long axis. We validated this approach by performing EA-TIRFM and radial sector analysis of in vitro actin filaments stabilized with Alexa 488–phalloidin, where the emission dipole is aligned along the filament axis (18) (Fig. S1 *D* and *E*).

The FA orientation vs. anisotropy data for αV-GFP–constrained was well fit by the $\cos^2$ function with an amplitude $A = 0.065 \pm 0.008$ and $\theta_d = -24.3 \pm 2.86°$, suggesting that GFP dipoles on αV-GFP–constrained are coaligned at this angle relative to the FA long axis (Fig. 1*E* and Table S1). In contrast, similar radial sector analysis for αV-GFP–unconstrained or CAAX-GFP showed much lower amplitudes of anisotropy vs. FA orientation data (Fig. 1*E* and Table S1). The orientation of the GFP dipole with respect to the FA long axis of αV-GFP–constrained derived from EA-TIRFM was verified using Instantaneous FluoPolScope (14), which indicated a dipole orientation of −19.5° ± 3.85° relative to the FA long axis (Fig. 1*F*). Thus, αVβ3 integrins are sterically constrained and organized in an anisotropic fashion, coaligned with one another, and specifically oriented relative to the FA long axis.

αV Integrin Alignment in FAs Requires Engagement to Immobilized Ligand. To test the role of ligand binding in αvβ3 integrin alignment, we plated cells expressing αV-GFP–constrained and paxillin-mCherry on either poly-L-lysine (PLL) to mediate nonspecific cell adhesion (19) or laminin that is not an αvβ3 ligand (20). TIRFM images of paxillin-mCherry showed that PLL inhibited FA formation, although rapid FN secretion by MEFs precluded complete FA abolition, while MEFs on laminin had robust paxillin-containing FA with poor enrichment of αV-GFP–constrained (Fig. 2*A*). Immunolocalization of the extended conformation of β3 integrin with LIBS2 antibody confirmed that PLL or laminin reduced αvβ3 integrin extension compared with FN (Fig. S4*E*). EA-TIRFM images of cells on PLL showed that anisotropy was low throughout the basal cell surface, with slightly higher or lower values in remnant FAs, while on laminin, anisotropy was at a high level throughout the basal cell surface, independent of location inside or outside of FAs (Fig. S3*C*). Radial sector analysis showed that, unlike cells plated on FN where anisotropy varied strongly as a function of FA orientation, in cells plated on PLL or laminin, the amplitude of the anisotropy vs. FA orientation data were similar to that of αV-GFP–unconstrained (Fig. 2*B*). Our results show that αV integrin alignment in FAs requires specific ligand binding and suggests crosstalk between laminin and FN receptors.

To determine whether integrin extension was sufficient for coalignment, cells expressing αV-GFP–constrained were pretreated with 1 mM Mn^{2+} and plated on PLL to prohibit ligand binding (21). Cells spread and formed large peripheral FAs and small FAs throughout their ventral surfaces (Fig. 2*A*), and LIBS2 staining confirmed increased β3 extension compared with PLL alone (Fig. S4*E*). EA-TIRFM and radial sector analysis showed that Mn^{2+} treatment and PLL plating reduced the amplitude of modulation of anisotropy as a function of FA orientation compared with cells on FN (Fig. 2*B*). Thus, integrin extension is not sufficient for coalignment in FAs.

We tested the requirement for ligand immobilization in integrin coalignment by plating cells on supported lipid bilayers functionalized with biotin-RGD (RGD-SLBs) as a freely diffusing αVβ3 ligand. Here, αV-GFP–constrained and paxillin-mCherry formed mobile clusters with very low anisotropy, and cells did not spread (22) (Fig. 2*A* and Fig. S3*C*). Since the long axis of clusters could not be determined reliably, we analyzed anisotropy in clusters as a function of orientation of their closest leading edge (Fig. S5). This anisotropy vs. cell edge orientation data exhibited a very low amplitude of modulation (Fig. 2*B* and Figs. S3*C* and S5*C*), although because orientation was not referenced to the polarization excitation, θ_d was meaningless. Thus, binding immobilized ligand promotes integrin coalignment in FAs, but binding to mobile ligand or adopting the extended conformation is not sufficient for alignment.

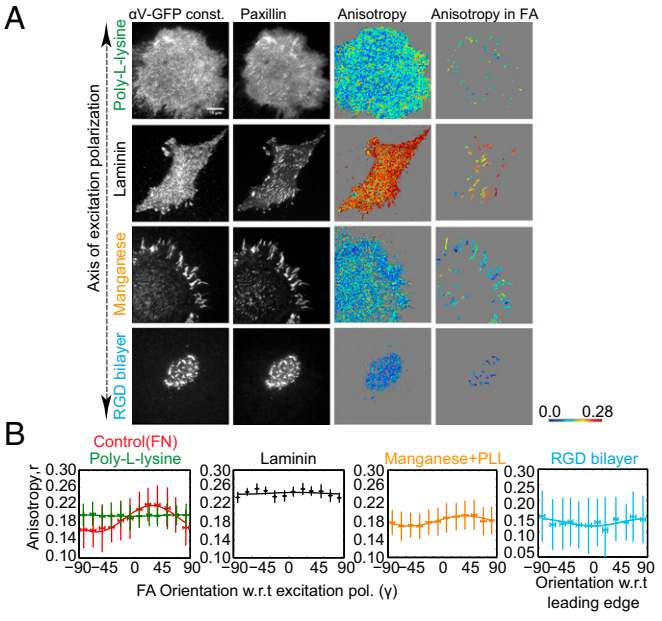

Fig. 2. αV integrin alignment in FAs requires binding to immobilized ligand. (*A*) Fluorescence images of αV-GFP–constrained (*Left*) or mApple-paxillin (*Left-Center*); *r* in cells (*Right Center*) and in FAs (*Right*) of MEF plated on PLL (*Top*), laminin (*Top Center*), pretreated with 1 mM Mn^{2+} and plated on PLL (*Bottom*, *Center*) or RGD-SLB (*Bottom*). Excitation polarization orientation (*Left*), anisotropy color scale (*Bottom*). (*B*) Average *r* in FAs vs. γ or orientation of a vector normal to the closest cell edge for αV-GFP–constrained, overlaid with fit to function in Fig. 1*D*. Error bars represent SEM. (Scale bar, 10 μm.)

αV Integrin Alignment Requires Talin-Mediated Linkage to an Intact, Flowing F-Actin Cytoskeleton. We next sought to determine the role of F-actin organization and dynamics in integrin alignment in FAs. We first asked whether F-actin and integrin alignment in FAs are related. EA-TIRFM and radial sector analysis of cells expressing αV-GFP–constrained and F-actin stained with Alexa 568–phalloidin showed that anisotropy vs. FA orientation data for both integrin and F-actin was well fit to the $\cos^2$ function, with different orientations of the dipoles with respect to the FA and greater dipole alignment (*A*) for F-actin than for αV-GFP–constrained (18) (Fig. 3 *A* and *B*, Fig. S4*A*, and Table S1). Plotting anisotropy of fluorescent phalloidin vs. that of αV-GFP–constrained in FAs showed a strong correlation (Fig. S4*C*). Thus, αV integrin and F-actin both align at FA.

We then tested the requirements for an intact F-actin cytoskeleton and the talin-mediated link between F-actin and integrins in promoting integrin alignment in FAs. In cells plated on FN, F-actin was disrupted by low-dose treatment with cytochalasin D (500 nM, 15 min) (Fig. 3 *C* and *D* and Fig. S4 *B* and *C*), while the integrin–F-actin link was inhibited by overexpressing the talin head domain tagged with mCherry (23) (Fig. 3 *E* and *F*). LIBS2 staining showed that, compared with control, disruption of F-actin reduced integrin extension, while talin head overexpression had little effect (Fig. S4*E*). SiR-655-actin, a far-red F-actin binding probe that has its dipole oriented differently with respect to the actin filament axis than that of fluorescent phalloidin (Fig. 3*F* and Fig. S4*D*), allowed simultaneous imaging of αV-GFP–constrained, talin head-mCherry, and F-actin. Phalloidin or SiR-actin staining and EA-TIRFM radial sector analysis of F-actin showed that cytochalasin disrupted the cytoskeleton and reduced F-actin anisotropy and its dependence on FA orientation (Fig. 3*D*, Fig. S4*B*, and Table S1), while talin head overexpression had no effect on F-actin morphology or anisotropy and its modulation (Fig. 3*F*). Despite these different effects on F-actin, both treatments attenuated αV-GFP–constrained anisotropy in FAs and its orientation dependence (Fig. 3 *D* and *F* and Table S1). Thus, although integrins and F-actin both align in FAs, F-actin alignment is not sufficient for integrin alignment. Instead, integrin alignment requires an intact cytoskeleton and is enhanced by the talin-mediated link between integrin and F-actin.

We then pursued the role of F-actin retrograde flow in integrin anisotropy and alignment. We first determined the speed and direction of F-actin flow in FAs by coexpressing paxillin-mApple and low levels of actin-GFP and performed TIR–fluorescent speckle microscopy (TIR-FSM) (24). Speckle flow-tracking algorithms (24) followed by plotting FA long axis vs. local F-actin flow orientation showed that F-actin flows along the FA long axis (Fig. 3*G*). Together with results above, this shows that integrin alignment is correlated with the direction of F-actin flow in FAs.

We next wanted to determine whether F-actin retrograde flow was required for integrin coalignment in FAs. As there is no reliable way to block all retrograde flow or alter its rate without disrupting F-actin integrity, we instead asked whether there was a regional correlation between F-actin flow and integrin alignment. We used the myosin-II inhibitor blebbistatin, which abolishes myosin-II–driven flow in the lamella and FAs, but leaves actin polymerization-driven flow and cytoskeletal integrity in the lamellipodium intact (25). As expected, blebbistatin eliminated cell polarity and blocked FA elongation, leaving a rim of diffraction-limited nascent adhesions (NAs) in lamellipodia (26) (Fig. 3*H*). EA-TIRFM of αV-GFP–constrained in blebbistatin-treated cells revealed higher levels of anisotropy in NA where retrograde flow remained intact, but very low levels in the cell interior where retrograde flow was blocked (25) (Fig. 3*I*). Since the long axis of NAs could not be determined, we analyzed anisotropy in NAs relative to the orientation of their closest leading edge (Fig. S5). This anisotropy vs. cell edge orientation data was well fit to the $\cos^2$ function, albeit with lower amplitude than untreated cells, although it had significantly higher amplitude than GFP-CAAX, αV-GFP–constrained in cells on PLL and αV-GFP–constrained on supported lipid bilayers (Fig. 3*J* and Fig. S5 *B* and *C*). Therefore, integrin coalignment in NAs spatially correlates with F-actin retrograde flow.

We wondered whether the loss of integrin coalignment induced by plating cells on PLL with or without Mn^{+2} or by overexpressing talin head could be due to effects of these perturbations on F-actin retrograde flow. TIR-FSM and speckle tracking analysis of F-actin dynamics showed that, for all three perturbations, F-actin underwent directed retrograde flow at enhanced speed compared with untreated cells (Fig. 3*K* and Movie S1). Together, these results show that F-actin retrograde flow spatially and directionally correlates with integrin alignment and suggests that integrin alignment requires binding immobilized ligand and a talin mediated linkage to a flowing cytoskeleton.

Modeling Integrin Orientation on the Cell Surface. We finally sought to model the absolute orientation of integrins in FAs on the cell

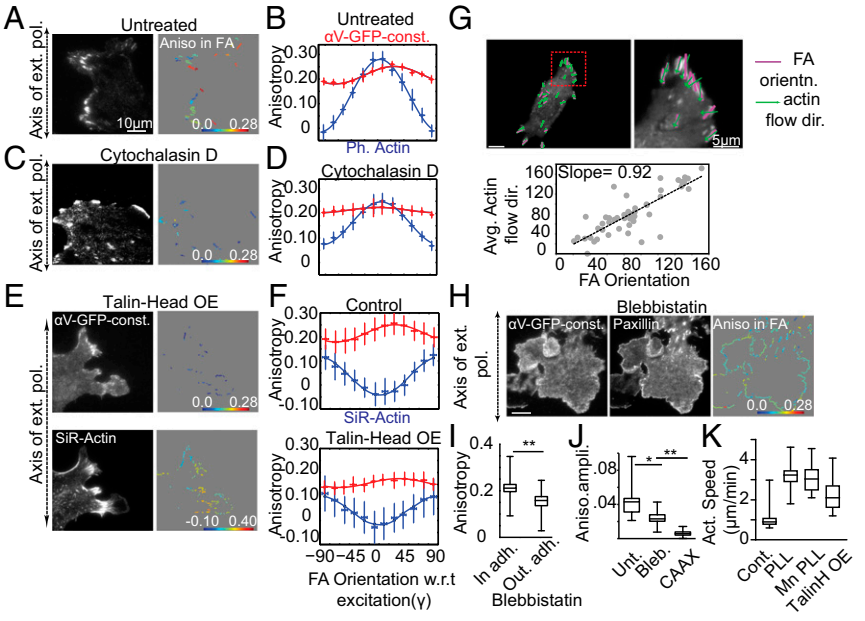

Fig. 3. αV integrin alignment in FAs requires talin-mediated linkage to a flowing F-actin cytoskeleton. (*A*, *C*, and *E*) Fluorescence images of αV-GFP–constrained (*A* and *C*, *Left*, and *E*, *Top Left*) or SiR-655-actin (*E*, *Bottom Left*); average *r* in FAs (*A*, *C*, and *E*, *Right*) untreated (*A*), 500 nM cyto D (*C*) overexpressing mCherry talin-head (*E*). Excitation polarization orientation (*Left*), anisotropy color scale (*Bottom*, also in *H*). (*B*, *D*, and *F*) Average *r* in FAs vs. γ for αV-GFP–constrained, conditions as in *A*, *C*, and *E*, overlaid with fit to function in Fig. 1*D*. Error bars represent SEM. (*G*, *Top*) Fluorescence images of mApple-paxillin overlaid with FA long axis (purple) and average F-actin flow vector (green), zoom at *Right*. (*G*, *Bottom*) Average F-actin flow direction in FAs vs. FA orientation relative to microscope *y* axis ($n = 50$ FAs, 5 cells), linear fit shown. (*H*) Fluorescence images of αV-GFP–constrained (*Left*) or mApple Paxillin (*Center*); average *r* in FAs (*Right*) of MEFs treated with 50 μM blebbistatin. (*I*) Average *r* of αV-GFP–constrained in nascent adhesions (in adh.) or cell interior (out adh.) for blebbistatin-treated cells. $n = 2{,}000$–$3{,}000$ ROI, 20 cells. (*J*) Amplitude (*A*) of anisotropy from the $\cos^2$ fit of anisotropy vs. orientation of a vector normal to the closest cell edge (Fig. S5) for αV-GFP–constrained control, blebbistatin-treated, or for GFP-CAAX. (*K*) F-actin retrograde flow speed in the periphery of MEFs expressing GFP-actin under conditions shown. $N = 50$–75 measurements, 5 cells per condition. (*I*, *J*, and *K*) Boxes include first quartile to third quartile, bar median, whiskers, min to max. $^*P < 0.001$; $^{**}P < 0.0001$, *H* test. (Scale bar, 10 μm.)

surface. Interpretation of integrin orientation in cells from the experimentally measured GFP dipole orientation in FAs required estimating the orientation of the GFP dipole with respect to integrin in our chimera, then "placing" the chimera in the frame of reference of the microscope with the dipole in the chimera oriented to match our measured dipole orientation in FAs. Because the measured dipole orientation is a 2D projection on the image plane of a dipole oriented in 3D, multiple orientations of αV-GFP–constrained can lead to a projection compatible with the measured orientation. To constrain the range of integrin orientations compatible with the measured orientation, we determined the GFP dipole orientation in FAs for a second chimera in which GFP was positioned differently relative to integrin than that in αV-GFP–constrained.

We generated αV-GFP–less-constrained by retaining the disordered N- and C-terminal portions of GFP and inserting at the same site in integrin as αV-GFP–constrained (27) (Fig. 4 *A* and *B*). EA-TIRFM and radial sector analysis of cells expressing αV-GFP–less-constrained showed that the anisotropy vs. FA orientation data was well fit to the $\cos^2$ function, albeit with a reduced amplitude compared with that of αV-GFP–constrained (Fig. 4*C* and Table S1), as expected from the longer linkers at the integrin-GFP junctions contributing to increased GFP mobility (Fig. 4*E*). The dipole was oriented at $\theta_d = -85.5° \pm 6.3°$ with respect to the FA long axis (confirmed using Instantaneous PolScope), distinct from the $\theta_d = -24.3 \pm 2.86°$ measured for αV-GFP–constrained.

To model the orientations of GFP relative to αVβ3 integrin for both chimeras, we used Rosetta (28). Integrin and GFP were treated as rigid bodies, and alternative conformations of the connecting segments at the integrin-GFP junctions that produced no steric clashes or strain in the linker region were sampled. Rosetta predicted an ensemble of permissible model structures for each chimera (Fig. 4*E*). A reference plane in the αVβ3 integrin was defined by three conserved positions in the integrin headpiece: Asp of the RGD ligand at the origin; and one at each junction between the headpiece and the αV and β3 legs. The orientation of the GFP dipole with respect to this plane was calculated for each model structure. This predicted a broader range of possible dipole orientations relative to the integrin for αV-GFP–less-constrained compared with that for αV-GFP–constrained, as expected (Fig. S6*A*).

To relate the measured GFP dipole orientations in FAs to integrin orientation in FAs, we created an integrin/microscope frame of reference (Fig. 4*F*). The *X*–*Y* plane was defined as parallel to the substrate/plasma membrane, with the FA long axis aligned along the *X* axis with +*X* toward the cell leading edge, the *X*–*Z* plane defined by the three conserved positions in the integrin headpiece, and the ligand-binding site pointed toward the substrate in the −*Z* direction along the optical axis (Fig. 4*F* and Fig. S6*B*).

We modeled the effect of rotating the integrin headpiece and ensemble of Rosetta structures associated with it around the integrin-ligand point in the integrin/microscope frame of reference on the projected dipole orientation in the image plane (Fig. S6 *C* and *D* and Movie S2). We assumed that the integrin was aligned with the line defined by the α-leg junction to β-leg junction along the FA (*X*) axis, as would be expected if tension were applied to the β-leg via retrograde flow. We determined the tilt (rotation around *Y* axis) of the integrin headpiece relative to the membrane that maximized the overlap between the dipole orientations in the projection of Rosetta models and the measured dipole orientations for both chimeras. We found that the maximum overlap is obtained when the headpiece is highly tilted (φ = 0–15°) toward the membrane plane (Fig. 4*H*). Considering our assumptions, the possible caveats of Rosetta modeling, and the broad spread in the possible orientations for αV–less-constrained, we speculate that the αVβ3 integrin headpiece is tilted relative to the membrane-normal (optical) axis along the axis of F-actin retrograde flow (Fig. 4*I*).

Discussion

Our results show that integrins can be ordered and aligned by the F-actin cytoskeleton. For decades, FAs have been described as "clusters" of integrin that recruit cytosolic FA-associated proteins. However, "cluster" implies no spatial ordering of proteins or framework for understanding the sensitivity of FAs to directional physical cues. Unlike F-actin, which is intrinsically ordered, ordering of integrins is actively imposed by extrinsic factors and correlates with conditions favoring directional F-actin motion and tension across the ligand–integrin–F-actin link, suggesting this factor is physical force. This is consistent with in vitro mixtures of F-actin and myosin II on SLBs where self-organization drives anisotropic clustering of membrane proteins (29).

Our results support a key prediction of the cytoskeleton force hypothesis for integrin activation (11): that linkage of integrins to F-actin retrograde flow through an adapter protein and activation and binding to a mechanically resistant ligand should orient and

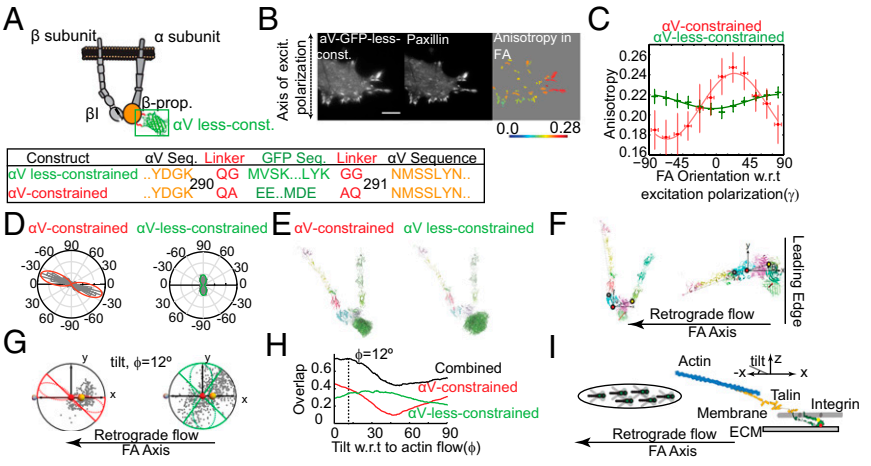

Fig. 4. αVβ3 integrin is predicted to have the legs tilted in the direction of retrograde flow. (*A*, *Top*) Schematic of αV-GFP–less-constrained in αVβ3 integrin. (*A*, *Bottom*) Amino acid sequences at GFP-αV integrin junctions. (*B*) Fluorescence images of αV-GFP–less-constrained (*Left*), mApple-paxillin (*Center*); average *r* in FAs (*Right*). Excitation polarization orientation (*Left*), anisotropy color scale (*Bottom*). (*C*) average *r* in FAs vs. γ for αV-GFP–constrained (red) and αV-GFP–less-constrained (green), overlaid with fit to function in Fig. 1*D*. Error bars represent SEM. (*D*) Histogram of GFP dipole orientation relative to FA long axis measured by Instantaneous FluoPolScope for αV-GFP–constrained and αV-GFP–less-constrained (n = 232 FAs, 11 cells); concentric circles: p; 0–0° axis: FA long axis; red, green outlines: circular Gaussian fits. (*E* and *F*) Ribbon diagrams of extended-open αVβ3 (*E*) ensembles of αv-GFP–constrained or αv-GFP–less-constrained chimeras output by Rosetta or (*F*) αV-GFP–constrained in the integrin/microscope frame of reference. GFP dipole: red arrow; integrin reference plane: spheres, ϕ: angle between αV-leg-junction-to-origin axis and *Z* axis; Θ: angle between projection of αV-leg-junction-to origin-axis on *X*–*Y* plane and *Z* axis; reference state: $\phi = 90°$ and $\Theta = 0°$. (*G*) Projection (onto the *X*–*Y* microscope plane) of GFP dipole orientations w.r.t. integrin headpiece from Rosetta models (gray point = one model) on a unit sphere at $\phi = 12°$. Dipole orientation, line from model to origin; p, length of line. Spheres are as in *F*. Dashed outlines: circular Gaussian fits; solid red, green outlines: FWHM of circular Gaussian. (*H*) Fraction of Rosetta models that lie within the angular range defined in *G* as a function of ϕ, in degrees when $\Theta = 0°$ for αV-GFP–constrained (red), αV-GFP–less-constrained (green), and their sum (black). Dotted line, value of ϕ at peak overlap. (*I*) Model of integrin alignment in FA (*Left*: along microscope *Z* axis) and of integrin, talin, and F-actin in FA (*Right*, view microscope *Y* axis). (Scale bar, 10 μm.)

align activated integrins in FAs. We show that alignment of αvβ3 integrins in FAs requires binding to β3-specific, immobilized ligand, and that F-actin alignment in stress fibers is not sufficient for integrin alignment, but requires coupling to F-actin via talin. Local inhibition of myosin-II–dependent retrograde flow in the lamella revealed a spatial correlation of integrin alignment with remaining flow in lamellipodia, supporting the notion that retrograde flow drives alignment. Lamellipodia consist of branched networks in which F-actin has a broad range of orientations relative to the cell edge (30), further supporting the notion that integrin ordering in lamellipodia is not templated by F-actin, but rather driven by F-actin flow. Together, this strongly suggests that the talin-mediated linkage between flowing F-actin and activated integrins bound to immobilized ligand actively orients and aligns integrins in FAs.

By using different GFP-tagged integrins and Rosetta modeling, our results suggest that activated, ligand-bound integrins are not erect on the cell surface as has been assumed, but may be tilted more parallel to the membrane along the direction of F-actin flow. Tilting of integrins on the cell surface was predicted using molecular-dynamics simulation to model integrin conformations in the presence of lateral forces, and may be allowed by the flexible residues connecting the extracellular domains and transmembrane domains (11). The tilt of integrins described here is similar to the tilts of both F-actin and talin in FAs (31, 32), suggesting force coaligns the integrin–talin–F-actin link (Fig. 4*I*). Additionally, the coalignment and tilting of integrins is not specific for αVβ3 or other FN binding integrins, as a concurrent study shows a similar organization for the LFA-1/αLβ2 integrins in migrating T cells (33, 34).

We speculate that integrins are strain sensors whose activation by force lies at the core of FA-mediated mechanotransduction. Integrins that happen to be oriented properly relative to applied force may be "chosen" for activation and ligand engagement, while misoriented integrins either remain inactive or, if already active, dissociate from ligand (11). This is consistent with the observation that stretch induces disassembly of FAs oriented perpendicular to the strain vector and growth of FAs parallel to the strain (35). Such force-induced activation of oriented integrins could mediate direction-dependent mechanosensing that promotes cell polarization in response to stretch and/or blood flow in the vasculature.

This work with previous studies show that FAs are built on an anisotropic molecular scaffold with distinct protein strata along their 150-nm thickness that sterically limits the possible interactions between FA proteins (36). The architecture of this scaffold prohibits a small protein like vinculin from simultaneously binding paxillin near the membrane and F-actin 120 nm away (37). Integrin alignment imposes an additional tier of steric regulation by orienting faces of the cytoplasmic tails relative to each other, thus constraining access of binding proteins to dimerization domains or other proteins. Force-dependent organization of the FA scaffold may thus sterically dictate specific protein interactions depending on the force magnitude to mediate mechanosensitive changes in FA signaling that drive distinct downstream cell behaviors.

ACKNOWLEDGMENTS. We thank Nikon and Andor Technology for imaging equipment and the Marine Biological Laboratory (MBL) Physiology Course students (2012, 2013) for preliminary results. This work was supported by Lillie Research award from MBL/University of Chicago (to C.M.W., T.A.S., S.M., and T.T.), NIH Grant 5R13GM085967 (Physiology Course at MBL), Howard Hughes Medical Institute Summer Institute at MBL (S.M.), NIH Grant CA31798 (to T.A.S., P.N., and T.I.M.), NIH Grant GM100160 (to T.T. and S.B.M.), NIH Grant GM092802 (to D.A.B. and N.K.), NIH Grant GM114274 (to R.O. and S.B.M.), Human Frontier Science Program (HFSP) Grant LT000096/2011-C (to S.B.M.), HFSP Grant RGP0027/2012, J. C. Bose and Wellcome Trust (S.M. and J.M.K.), and National Heart, Lung, and Blood Institute Division of Intramural Research (C.M.W. and V.S.).

1. Hynes RO (2002) Integrins: Bidirectional, allosteric signaling machines. *Cell* 110:673–687.
2. Moser M, Legate KR, Zent R, Fässler R (2009) The tail of integrins, talin, and kindlins. *Science* 324:895–899.
3. Zaidel-Bar R, Itzkovitz S, Ma'ayan A, Iyengar R, Geiger B (2007) Functional atlas of the integrin adhesome. *Nat Cell Biol* 9:858–867.
4. Hoffman BD, Grashoff C, Schwartz MA (2011) Dynamic molecular processes mediate cellular mechanotransduction. *Nature* 475:316–323.
5. Davies PF (1995) Flow-mediated endothelial mechanotransduction. *Physiol Rev* 75:519–560.
6. Lauffenburger DA, Horwitz AF (1996) Cell migration: A physically integrated molecular process. *Cell* 84:359–369.
7. Levental KR, et al. (2009) Matrix crosslinking forces tumor progression by enhancing integrin signaling. *Cell* 139:891–906.
8. Parsons JT, Horwitz AR, Schwartz MA (2010) Cell adhesion: Integrating cytoskeletal dynamics and cellular tension. *Nat Rev Mol Cell Biol* 11:633–643.
9. Pollard TD, Blanchoin L, Mullins RD (2000) Molecular mechanisms controlling actin filament dynamics in nonmuscle cells. *Annu Rev Biophys Biomol Struct* 29:545–576.
10. Chan CE, Odde DJ (2008) Traction dynamics of filopodia on compliant substrates. *Science* 322:1687–1691.
11. Zhu J, et al. (2008) Structure of a complete integrin ectodomain in a physiologic resting state and activation and deactivation by applied forces. *Mol Cell* 32:849–861.
12. Lakowicz JR (1999) Fluorescence anisotropy. *Principles of Fluorescence Spectroscopy* (Springer, Boston), pp 291–319.
13. Shi X, et al. (2007) Ultrafast excited-state dynamics in the green fluorescent protein variant S65T/H148D. 2. Unusual photophysical properties. *Biochemistry* 46:12014–12025.
14. Mehta SB, et al. (2016) Dissection of molecular assembly dynamics by tracking orientation and position of single molecules in live cells. *Proc Natl Acad Sci USA* 113:E6352–E6361.
15. Rocheleau JV, Edidin M, Piston DW (2003) Intrasequence GFP in class I MHC molecules, a rigid probe for fluorescence anisotropy measurements of the membrane environment. *Biophys J* 84:4078–4086.
16. Shibata ACE, et al. (2012) Archipelago architecture of the focal adhesion: Membrane molecules freely enter and exit from the focal adhesion zone. *Cytoskeleton* 69:380–392.
17. Rossier O, et al. (2012) Integrins β1 and β3 exhibit distinct dynamic nanoscale organizations inside focal adhesions. *Nat Cell Biol* 14:1057–1067.
18. Fishkind DJ, Wang YL (1993) Orientation and three-dimensional organization of actin filaments in dividing cultured cells. *J Cell Biol* 123:837–848.
19. Schlaepfer DD, Hanks SK, Hunter T, van der Geer P (1994) Integrin-mediated signal transduction linked to Ras pathway by GRB2 binding to focal adhesion kinase. *Nature* 372:786–791.
20. Ramovs V, Te Molder L, Sonnenberg A (2017) The opposing roles of laminin-binding integrins in cancer. *Matrix Biol* 57–58:213–243.
21. Takagi J, Petre BM, Walz T, Springer TA (2002) Global conformational rearrangements in integrin extracellular domains in outside-in and inside-out signaling. *Cell* 110:599–11.
22. Yu C-H, Law JBK, Suryana M, Low HY, Sheetz MP (2011) Early integrin binding to Arg-Gly-Asp peptide activates actin polymerization and contractile movement that stimulates outward translocation. *Proc Natl Acad Sci USA* 108:20585–20590.
23. Calderwood DA, et al. (1999) The talin head domain binds to integrin β subunit cytoplasmic tails and regulates integrin activation. *J Biol Chem* 274:28071–28074.
24. Vallotton P, Ponti A, Waterman-Storer CM, Salmon ED, Danuser G (2003) Recovery, visualization, and analysis of actin and tubulin polymer flow in live cells: A fluorescent speckle microscopy study. *Biophys J* 85:1289–1306.
25. Gardel ML, et al. (2008) Traction stress in focal adhesions correlates biphasically with actin retrograde flow speed. *J Cell Biol* 183:999–1005.
26. Choi CK, et al. (2008) Actin and alpha-actinin orchestrate the assembly and maturation of nascent adhesions in a myosin II motor-independent manner. *Nat Cell Biol* 10:1039–1050.
27. Vrabioiu AM, Mitchison TJ (2006) Structural insights into yeast septin organization from polarized fluorescence microscopy. *Nature* 443:466–469.
28. Rohl CA, Strauss CEM, Misura KMS, Baker D (2004) Protein structure prediction using Rosetta. *Methods Enzymol* 383:66–93.
29. Köster DV, et al. (2016) Actomyosin dynamics drive local membrane component organization in an in vitro active composite layer. *Proc Natl Acad Sci USA* 113:E1645–E1654.
30. Svitkina TM, Verkhovsky AB, McQuade KM, Borisy GG (1997) Analysis of the actin-myosin II system in fish epidermal keratocytes: Mechanism of cell body translocation. *J Cell Biol* 139:397–415.
31. Liu J, et al. (2015) Talin determines the nanoscale architecture of focal adhesions. *Proc Natl Acad Sci USA* 112:E4864–E4873.
32. Abercrombie M, Heaysman JE, Pegrum SM (1971) The locomotion of fibroblasts in culture. IV. Electron microscopy of the leading lamella. *Exp Cell Res* 67:359–367.
33. Nordenfelt P, et al. (2016) Direction of actin flow dictates integrin LFA-1 orientation during leukocyte migration. bioRxiv:10.1101/071936.
34. Swaminathan V, et al. (2016) Actin retrograde flow actively aligns and orients ligand-engaged integrins in focal adhesions. bioRxiv:10.1101/071852.
35. Chen Y, Pasapera AM, Koretsky AP, Waterman CM (2013) Orientation-specific responses to sustained uniaxial stretching in focal adhesion growth and turnover. *Proc Natl Acad Sci USA* 110:E2352–E2361.
36. Kanchanawong P, et al. (2010) Nanoscale architecture of integrin-based cell adhesions. *Nature* 468:580–584.
37. Case LB, et al. (2015) Molecular mechanism of vinculin activation and nanoscale spatial organization in focal adhesions. *Nat Cell Biol* 17:880–892.
38. Bonasio R, et al. (2007) Specific and covalent labeling of a membrane protein with organic fluorochromes and quantum dots. *Proc Natl Acad Sci USA* 104:14753–14758.
39. Mattheyses AL, Kampmann M, Atkinson CE, Simon SM (2010) Fluorescence anisotropy reveals order and disorder of protein domains in the nuclear pore complex. *Biophys J* 99:1706–1717.
40. Axelrod D (1979) Carbocyanine dye orientation in red cell membrane studied by microscopic fluorescence polarization. *Biophys J* 26:557–573.